The 1990 to 1991 Sudan Earthquake Sequence and the Extent of the East African Rift System

R. W. Girdler* and D. A. McConnell

One of the largest earthquakes ever recorded in Africa (surface wave magnitude M_s = 7.2) occurred about 50 kilometers east of the Upper River Nile on 20 May 1990. Four days later, two more large earthquakes (M_s = 6.4 and 7.0) occurred about 50 kilometers to the northwest in the Nile Valley. In the following months, a further 60 events were recorded by seismic stations worldwide. The earthquakes are associated with two fault systems: one east of the Nile with azimuth southeast and one along the Nile Valley with azimuth north-northeast. The activity alternated between the two fault systems and indicates that the northern extremity of the western branch of the East African Rift System extends at least 350 kilometers north of Lake Albert.

The northernmost extremity of the western branch of the East African Rift System (Fig. 1) is usually considered to be Lake Albert (Mobutu) and the Albert Nile (*1–3*). Lake Albert occupies a 60-km-wide northeast-trending rift valley (*4*); the Albert Nile drains its northernmost corner. At 3.7°N, the Nile is deflected by and follows the 560- to 790-million-year-old northwest Aswa shear zone (*5, 6*) for about 70 km before continuing north-northeast as the White Nile. At 5.6°N, it is again deflected northwest along a possible parallel shear zone. It is in this region on 20 May 1990 that a large earthquake occurred (M_s = 7.2), causing damage in southern Sudan and shaking parts of Uganda and Kenya. It is believed to be the largest earthquake ever recorded in the Sudan (*7*).

A total of 64 earthquakes in this area between May 1990 and September 1991 are documented in the world listings (*7, 8*). These events have been numbered from 1 to 64; International Seismological Centre (ISC) data are available for events 1 to 62, and National Earthquake Information Service (NEIS) data for 63 and 64. We relocated events 1 to 49 using the method of joint epicenter determination (JED) (*9, 10*). Relocation involves selecting and restraining a master event (usually the largest) and then relocating nearby events with reference to the fixed master. The relative positions with respect to the restrained master have a better accuracy, thus facilitating recognition of structures with which the earthquakes might be associated.

The six largest events were 1, 6, 7, 37, 44, and 48 (Table 1). Fault plane solutions [Harvard centroid-moment tensor solutions (*11–13*)] show that event 1, 45 km east of the Nile, is associated with left-lateral shear; events 6 and 7, on the east bank of the Nile, are associated with dominantly normal faulting with dips northwest; and events 37 and 48, on the west bank, are associated with dominantly normal faulting with dips southeast, consistent with the Nile flowing through a rift valley in this region. Event 44, nearly 100 km east of the Nile, also shows normal faulting.

Arranging the events for relocation revealed that the seismic activity alternated between two regions: one to the east of the Nile and the other along the Nile Valley about 50 km to the northwest (Fig. 2). Events 1 to 5, 24 to 31, and 38 to 47 were east of the Nile, and events 6 to 23, 32 to 37, and 48 were in or near the Nile Valley. Over the next 12 months the activity became spasmodic, with one event in September 1990, one in December, four in January 1991, two in February, five in March, one in May, and two in September. With the exception of event 61, all of these were widely scattered to the east of the Nile. It seems the large earthquake on 20 May (event 1), 50 km east of the Nile, triggered activity on faults along the Nile Valley, after which the activity mostly alternated between the two regions before finally dying out on the east side.

Subsequence 1 (events 1 to 5, 20 to 23 May 1990). Event 1, the largest, originated at and resulted from left-lateral shear along a fault with azimuth 136° and dip 86° southwest (*12*). The Aswa shear zone and a number of lineations in the region have similar trend [(*14*) and Landsat imagery]. Events 1, 3, and 5 were most likely along the same fault, but the confidence ellipses (Fig. 2B) for events 2 and 4 suggest that these could have been associated with faulting to the south.

Subsequence 2 (events 6 to 23, 24 May to 4 June 1990). These were associated with the Nile Valley, with the exception of event 21. The largest events, 6 (body magnitude m_b = 5.9, M_s = 6.4) and 7 (m_b = 6.4, M_s = 7.0), occurred only 24 min apart on 24 May on the east side of the valley (Fig. 2B). The earthquake mechanisms show normal faulting with azimuth 52° to 56° and dip 39° to 43° northwest (*12*). These mechanisms are consistent with the motion vectors for event 1 (southeast shear), implying increasing tension in the Nile Valley that could have triggered these events. Most were aligned north-northeast on the east side of the valley, but events 11 to 14, 17, and 22 were more scattered on the west side, suggestive of the commencement of activity on another fault on the other side of the valley.

Subsequence 3 (events 24 to 31, 3 to 19 June 1990). Over the next 16 days, activity returned to the plains east of the Nile. Events 24, 27, 28, and 29 occurred to the northwest of events 1, 3, and 5 (subsequence 1), possibly along the same fault. Events 26 and 30 were to the south, possibly along parallel shears.

Subsequence 4 (events 32 to 37, 20 June to 9 July 1990). On 20 June, activity returned to the Nile Valley but this time was mostly on the west side (the one exception was event 34, which, like 21 of subsequence 2, was far to the east). Instead of large events with aftershocks, there was a buildup of activity (Fig. 2A) culminating in the third largest event (event 37) on 9 July (m_b = 5.9, M_s = 6.4), which was recorded by the second largest number of stations

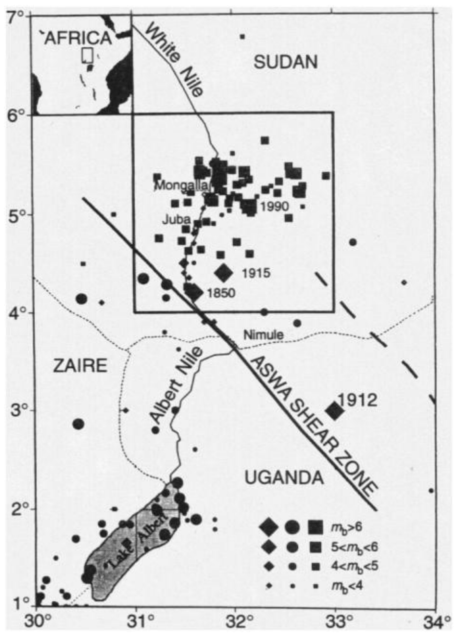

Fig. 1. Seismicity of the northernmost part of the western branch of the East African Rift System. The 1990–1991 Sudan earthquakes (squares) are mostly north of 5°N. Diamonds: epicenters from 1850 through 1963; circles and squares: ISC epicenters from 1964 through May 1991 and NEIS epicenters from June 1991 through April 1993. Most have an accuracy of about 10 km. Historical seismicity (*7, 20, 21*) is also shown, these locations being less accurate.

Department of Physics, University of Newcastle upon Tyne, Newcastle upon Tyne, NE1 7RU, United Kingdom.

*To whom correspondence should be addressed.

(534). The earthquake mechanism (azimuth 28°, dip 44° southeast) is consistent with normal faulting on the west side of the valley (*13*).

Subsequence 5 (events 38 to 47, 13 July to 13 August 1990). Over the next month, the activity became more scattered in time and space and was confined to the region east of the Nile. These events were most likely associated with the northwest-southeast shear zones.

Subsequence 6 (event 48, 9 September 1990). There was one more event in the Nile Valley (m_b = 5.2 and M_s = 5.3, recorded by 273 stations). It was located close to the large event 37 on the west side of the valley and had a similar earthquake mechanism (azimuth 44°, dip 43° southeast) (*13*). There have been no further large events in the valley, and subsequent events have been mostly small and widely scattered in the plains to the east.

The earthquake mechanisms and their JED relocations support the view first suggested by Holmes (*15, 16*) in 1916 that the Nile here is flowing through a rift valley. The two pairs of events (6 and 7 and 37 and 48) were on opposite sides of the valley about 20 to 30 km apart. If these were associated with the major faults, the rift here is somewhat narrower than the Albert rift to the south, which is about 50 km wide and has a similar northeast trend. Least squares lines fitted to the epicenters on the east and west sides give azimuths 25° ± 7°N and 25° ± 6°N, respectively (Fig. 3A). This assumes that there is only one rift fault on either side; it is, of course, possible there

Table 1. Largest events of the earthquake sequence. *H*, focal depth; *N*, number of stations recording each earthquake. Data from ISC.

Event	Date	Time (UT)	Location °N	Location °E	*H* (km)	m_b	M_s	*N*
1	20 May	02:22:01.2	5.07	32.16	13	6.5	7.2	639
6	24 May	19:34:47.0	5.33	31.84	24	5.9	6.4	513
7	24 May	20:00:08.2	5.36	31.87	20	6.4	7.0	521
37	9 July	15:11:20.4	5.45	32.67	16	5.9	6.4	534
44	28 July	16:46:04.0	5.22	32.65	16	5.4	5.1	271
48	7 Sep	00:12:26.2	5.43	31.66	14	5.2	5.3	273

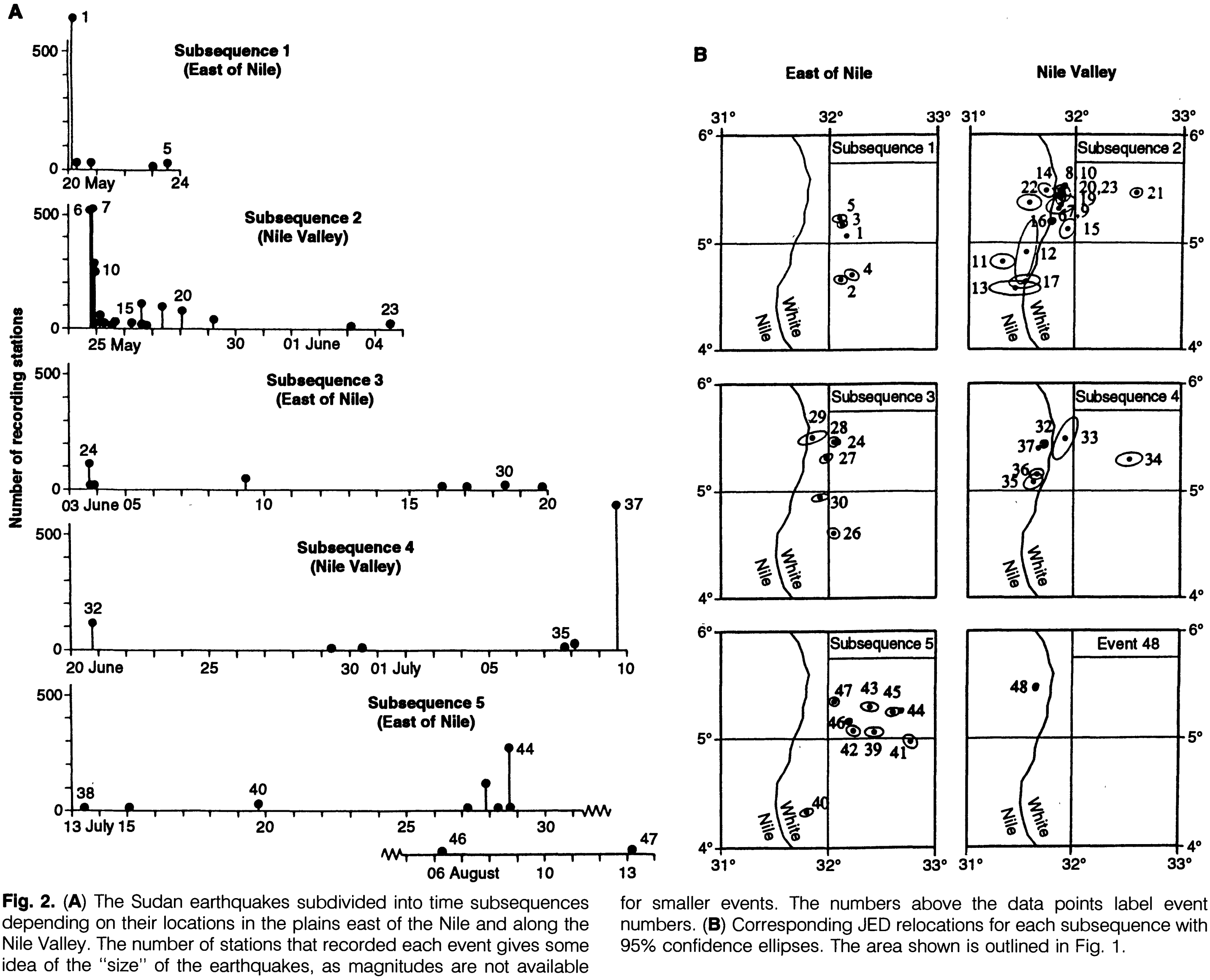

Fig. 2. (**A**) The Sudan earthquakes subdivided into time subsequences depending on their locations in the plains east of the Nile and along the Nile Valley. The number of stations that recorded each event gives some idea of the "size" of the earthquakes, as magnitudes are not available for smaller events. The numbers above the data points label event numbers. (**B**) Corresponding JED relocations for each subsequence with 95% confidence ellipses. The area shown is outlined in Fig. 1.

is more than one fault, especially on the west side.

The events in the plains to the east of the Nile (Fig. 3B) were very much more scattered than those associated with the Nile Valley. The left-lateral shear mechanism for event 1 suggests a structure parallel to the Aswa shear zone. It is much more difficult to relate these epicenters to specific faults (*17*). Several northwest-southeast features can be seen north of the Aswa shear zone on a map traced from Landsat imagery (Fig. 4). These become less clear as the Nile is approached. One such feature can be seen due southeast of event 1 but not running through it, possibly being obscured by the savanna terrain. It seems likely that there are several unrecognized shear zones 100 to 200 km north of the well-known Aswa shear zone.

This seismic activity suggests that the course of the Upper Nile (Bahr el Jebel) is fault-controlled. The character of the Upper Nile (*18*) changes depending on whether it is flowing north-northeast or northwest. From Lake Albert to Nimule (Fig. 1), it is a placid stream, fringed by swamp, flowing in a well-defined valley with a maximum width of 6 km (rift structure). At Nimule, it is deflected northwest along the Aswa shear zone and becomes a rocky stream with rapids confined within a narrow valley. At about 4.2°N, it again flows north-northeast and becomes navigable some distance south of Juba, meandering and braided in a well-defined valley. This is the rift structure (Fig. 3A) along which earthquake subsequences 2, 4, and 6 occurred (Fig. 2). A topographic map of the Juba region (*19*) shows hot springs on the east bank at 4.25°N, indicating that this part of the rift has high heat flow. Finally, at about 5.75°N, the river is again deflected and flows northwest for about 360 km along the proposed shear zone where event 1 occurred. Tributaries of the Nile, that is, the Son and Koss (Fig. 4), flow along this shear zone to join the Nile at about 5.7°N, 31.8°E. The geometry is similar to the way in which the Aswa River flows northwest along the Aswa shear zone to join the Nile at 2.7°N, 32°E. The seismic activity indicates that the western branch of the East African Rift System propagates at least as far north as 5.5°N.

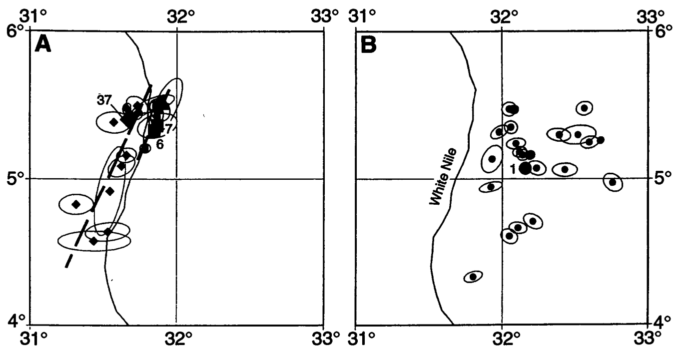

Fig. 3. (**A**) JED relocated events in the Nile Valley: Squares indicate events on the east bank (master events 6 and 7), and diamonds mark events on the west bank (master event 37). Possible normal faults (least squares lines fitted through the epicenters) are shown by dashed lines. (**B**) JED relocated events (circles) in the plains to the east of the Nile (master event 1).

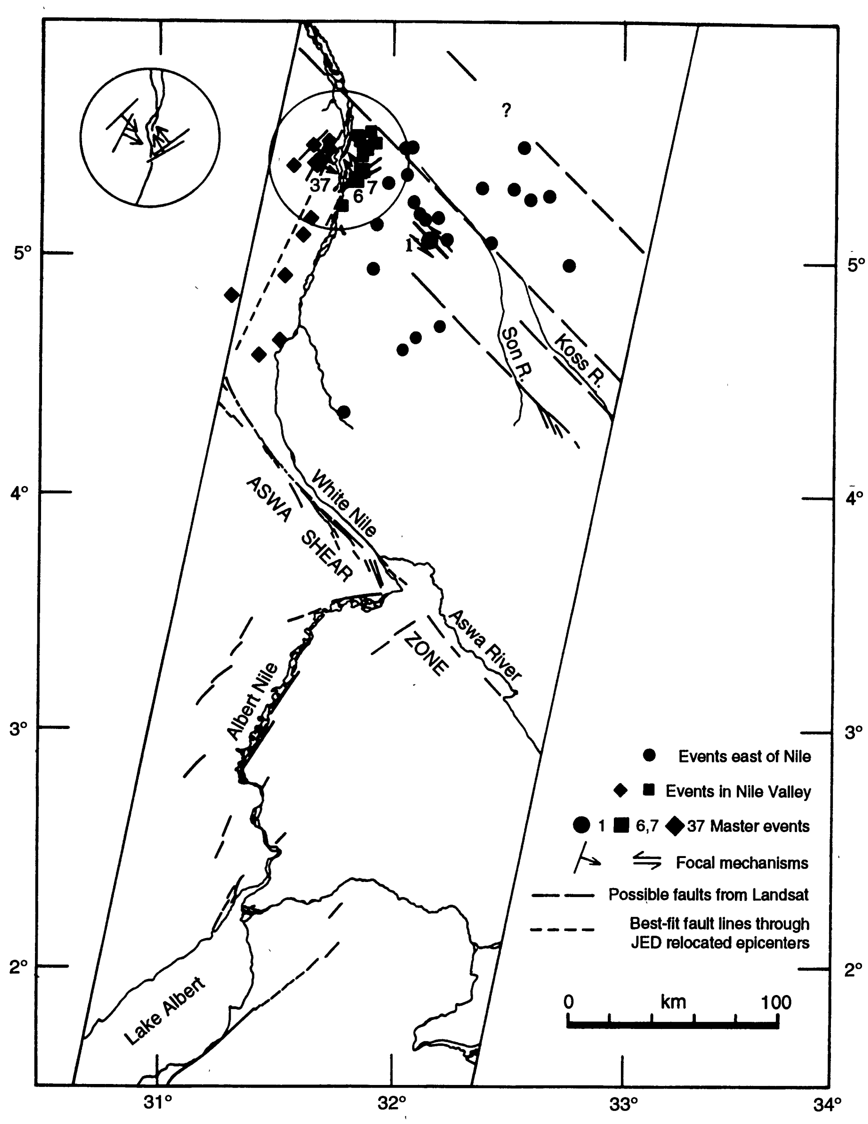

Fig. 4. The 1990–1991 Sudan earthquake sequence (JED relocations) plotted on a tracing from Landsat imagery (satellite path indicated by north-northeast parallel lines) showing the possible normal faults along the Nile Valley inferred from the earthquakes and the possible strike-slip faults in the plains to the east of the Nile inferred from the satellite imagery. (**Inset**) Details of fault plane solutions for the Nile Valley.

REFERENCES AND NOTES

1. *UNESCO International Tectonic Map of Africa* (UNESCO Earth Sciences, Paris, France, 1968).
2. J. D. Fairhead and R. W. Girdler, *Geophys. J. R. Astron. Soc.* **24**, 271 (1971).
3. B. R. Rosendahl, *Annu. Rev. Earth Planet. Sci.* **15**, 445 (1987).
4. Geological Survey of Uganda, *Geological Map of Uganda with Bouguer Gravity Anomalies* (scale 1:250,000) (Lands and Surveys Department, Uganda, 1961).
5. J. V. Hepworth and R. Macdonald, *Nature* **210**, 726 (1966).
6. L. Cahen, N. J. Snelling, J. Delhal, J. R. Vail, *The Geology and Evolution of Africa* (Clarendon, Oxford, 1984).
7. International Seismological Centre, *Historical Hypocentre Data File (1904–1991)* (Newbury, United Kingdom).
8. National Earthquake Information Center, *Preliminary Determination of Epicenters 1990–1991* (U.S. Geological Survey, Boulder, CO, 1992).
9. A. Douglas, *Nature* **215**, 47 (1967). For the relocations, event 1 was used as the master for events east of the Nile, events 6 and 7 as joint masters for events on the east bank of the Nile,

and event 37 for events on the west bank. All the masters were recorded by more than 500 stations.
10. A. Douglas, R. C. Lilwall, J. B. Young, *Atomic Weapons Research Establishment Report O 28/74 MOD Procurement Exec.* (Her Majesty's Stationary Office, London, 1972).
11. A. M. Dziewonski, G. Ekstrom, J. E. Franzen, J. H. Woodhouse, *Phys. Earth Planet. Inter.* **45**, 1 (1987).
12. ———, *ibid.* **66**, 133 (1991).
13. ———, *ibid.* **67**, 210 (1991).
14. Geological Survey of Sudan, *Geological Map of the Sudan* (scale 1:2,000,000) (Geological and Mineral Resources Department, Khartoum, Sudan, 1981).
15. A. Holmes, *Geogr. J.* **48**, 149 (1916).
16. C. H. Stigand, *ibid.*, p. 145.
17. R. Gaulon, J. Chorowicz, G. Vidal, B. Romanowicz, G. Roult, *Tectonophysics* **209**, 87 (1992).
18. H. E. Hurst and P. Phillips, *General Description of the Basin, Meteorology, Topography of the White Nile Basin*, vol. 1 of *The Nile Basin* (Government Press, Cairo, Egypt, 1931).
19. War Office, *Juba Zone G Topographic Map Sheet N.B. 36/4* (scale 1:500,000) (Geographical Section General Staff No. 4355, Sudan, 1947).
20. N. N. Ambreseys and R. D. Adams, *Bull. Seismol. Soc. Am.* **76**, 483 (1986).
21. B. Gutenberg and C. F. Richter, *Seismicity of the Earth* (Princeton Univ. Press, Princeton, NJ, 1954).
22. We thank P. Davis, A. Douglas, J. Young, D. Jackson, J. Heirtzler, and D. Morgan for assistance and the Atomic Weapons Research Establishment Seismological Research Unit (Blacknest, United Kingdom), International Seismological Centre (Newbury, United Kingdom), the Department of Earth and Space Sciences at the University of California, Los Angeles (California), NASA/Goddard Space Flight Center (Greenbelt, Maryland), and the Geography Department at the University of Durham (Durham, United Kingdom) for logistical support.

28 September 1993; accepted 24 January 1994

El Niño on the Devil's Staircase: Annual Subharmonic Steps to Chaos

Fei-Fei Jin, J. David Neelin,* Michael Ghil

The source of irregularity in El Niño, the large interannual climate variation of the Pacific ocean-atmosphere system, has remained elusive. Results from an El Niño model exhibit transition to chaos through a series of frequency-locked steps created by nonlinear resonance with the Earth's annual cycle. The overlapping of these resonances leads to the chaotic behavior. This transition scenario explains a number of climate model results and produces spectral characteristics consistent with currently available data.

El Niño, the name given by Peruvian fishermen to an aperiodic warming of equatorial surface waters—now known to affect much of the globe (*1*)—refers to the Christ child because in years when it occurs, coastal manifestations tend to appear around Christmas. A decade of research has led to a view of El Niño as an essentially cyclic phenomenon and to an understanding of the mechanisms that drive the oscillation between warm and cold phases and determine the spatial pattern (*2, 3*). Current major theoretical challenges are the interaction of El Niño with the seasonal cycle (*2*), which provided its saintly name, and the source of its devilishly irregular behavior. We as well as Tziperman and colleagues (*4*) show how the latter is caused by the former. The respective approaches complement each other because Tziperman and co-workers analyze the basics of the mechanism in a simple model, while our model provides fuller physical mechanisms, along with connections to other models. Our coupled ocean-atmosphere model (*5, 6*) is closely related to the Cane-Zebiak model used for operational predictions of El Niño (*7*). Ours has been used (*5*) to understand the relation among the flow regimes of many El Niño models (*7–14*) including complex coupled general circulation models and hybrid coupled models. This modeling pedigree is important because some earlier results on El Niño irregularity have arisen from numerical artifacts (*15*).

When the annual cycle is absent in El Niño models, the spatial pattern and inherent period of the interannual oscillations are determined by the nonlinear saturation of an oscillatory, unstable ocean-atmosphere mode. The instability involves feedbacks between the sea surface temperature (SST), which affects the atmospheric circulation, and the dynamics of the ocean circulation, in which currents and thermocline depth must adjust to the changes in wind. The resulting SST–ocean-dynamics modes have several regimes of behavior (*3*), mirrored in the differing behavior of several climate models (*12*). Observational evidence (*16, 17*) points to a regime in which the memory of the system is provided mainly by the time scale of subsurface adjustment by ocean dynamics, whereas the spatial form and growth mechanisms are largely independent of these time scales. The large spatial scale of El Niño and its atmospheric manifestation, the Southern Oscillation (together known as ENSO), arise because each medium responds in an integrating fashion to the anomalies of the other, favoring the growth of the largest scale mode. The oscillatory behavior occurs because the slowly adjusting ocean dynamics never quite catch up with the changes in the wind over the basin. A convenient metaphor for this process is known as the delayed-oscillator model (*4, 9, 13*). This simple model, with idealized wind anomalies depending on SST at a single point and truncated ocean dynamics, can be justified in terms of the mixed SST–ocean-dynamics modes of more complex models [see (*3*) for review] for significant portions of their respective bifurcation diagrams (*5*).

When the seasonal cycle is included in a coupled model with El Niño oscillations and no atmospheric noise, several things can happen: The motion can be quasiperiodic (that is, with two incommensurable frequencies, the inherent El Niño frequency and its annual modulation); the motion can be irregular; or the El Niño cycle can be entrained nonlinearly into synchrony with the annual cycle to form a periodic oscillation with a longer period—a subharmonic oscillation. We mapped this interaction of El Niño and the seasonal cycle systematically in our model and found it to be organized about a "devil's staircase"—a structure in which the inherent frequency of the system locks onto a sequence of rational fractions of the external frequency and that is associated with the transition to chaos by the overlapping of these nonlinear resonances (*18*).

The approximate devil's staircase in Fig. 1A is constructed from many 100-year runs of the model. We changed a parameter, δ_s, which determines the strength of anomalous currents and upwelling in the model's surface layer (*5*), to modify the inherent period of the model El Niño cycle. For stronger surface-layer feedbacks, zonal and vertical advection anomalies add to the time rate of change of SST caused by thermocline-depth anomalies. The most realistic regime for the model ENSOs occurs between values of about 0.2 and 0.4 on this nondimensional scale. We swept through a greater range of values to see the structure in which the realistic range is embedded, and because some climate models fall into the higher value range (*12*). Over much of the parameter range, the ENSO frequency is discretized into a series of frequency-locked steps (known as Arnold tongues) at rational fractions of the annual frequency. A complete devil's staircase has an infinite

F.-F. Jin, Department of Meteorology, University of Hawaii at Manoa, Honolulu, HI 96822, USA.
J. D. Neelin, Department of Atmospheric Sciences, University of California at Los Angeles, Los Angeles, CA 90024-1565, USA.
M. Ghil, Department of Atmospheric Sciences and Institute of Geophysics and Planetary Physics, University of California at Los Angeles, Los Angeles, CA 90024-1565, USA.

*To whom correspondence should be addressed.